A Femtosecond Visible/Visible and Visible/Mid-Infrared Transient Absorption Study of the Light Harvesting Complex II

Andreas D. Stahl, Mariangela Di Donato, Ivo van Stokkum, Rienk van Grondelle, and Marie Louise Groot*
Faculty of Sciences, Department of Physics and Astronomy, VU University Amsterdam, Amsterdam, The Netherlands

ABSTRACT Light harvesting complex II (LHCII) is the most abundant protein in the thylakoid membrane of higher plants and green algae. LHCII acts to collect solar radiation, transferring this energy mainly toward photosystem II, with a smaller amount going to photosystem I; it is then converted into a chemical, storable form. We performed time-resolved femtosecond visible pump/mid-infrared probe and visible pump/visible probe absorption difference spectroscopy on purified LHCII to gain insight into the energy transfer in this complex occurring in the femto-picosecond time regime. We find that information derived from mid-infrared spectra, together with structural and modeling information, provides a unique visualization of the flow of energy via the bottleneck pigment chlorophyll a604.

INTRODUCTION

The trimeric light harvesting complex II (LHCII) is the most abundant protein in the thylakoid membrane of higher green plants and green algae. Approximately 50% of the chlorophylls (Chls) in the thylakoid membrane are contained in the LHCII complex, which is mainly associated with the photosystem II (PSII). Since Thornber and Ogawa independently discovered LHCII >40 years ago (1,2), the complex has been the subject of intense study, using a broad variety of experimental techniques (3–6). LHCII acts to collect solar radiation and transfers this energy toward PSII and photosystem I (PSI) where it is converted into a chemical, storable form. LHCII thus acts as an antenna, directly increasing the effective absorption cross section of PSI and PSII by funneling energy toward them. It has also been established that LHCII contributes to photoprotection (7,8) and energy dissipation under high light conditions (9–12). In addition, LHCII is involved in regulating the distribution of absorbed energy between the two photosystems (13).

In the native form, LHCII is a trimer of three identical monomers, each with a mass of ~25 kDa. From the crystallographic data described in Liu et al. (14) with 2.72 Å resolution (and later on with 2.5 Å resolution in (15)), it is known that every monomer contains six chlorophyll *b* molecules, eight chlorophyll *a* molecules, and 232 amino-acid residues (see Fig. 1). Furthermore, four carotenoid binding sites were found, in which two luteins and one neoxanthin were unambiguously identified, but no precise assignment has been given for the fourth carotenoid, which is thought to be involved in the xanthophyll cycle. The LHCII carotenoids play a major role in the stabilization of the structure. A variety of studies, such as transient absorption, time-resolved fluorescence, and photon echo spectroscopies, have been performed to study the dynamics of excitation energy transfer within the LHCII complex. Chl-*b*-to-Chl-*a* transfer and transfer among Chl *a* pigments was found to occur with time constants of 150–300 fs, 600 fs, and 2–5 ps; however, a slower process taking place on a 10–20 ps timescale was also observed (6,16–26).

Additional information on the timescales and possible pathways of energy transfer has become available from application of a disordered exciton plus modified Redfield relaxation theory to LHCII, where knowledge of the structure, the effective dipole moments of Chls, and the spectral density of electron-phonon coupling is used to model steady-state spectra and time-resolved data at a quantitative level (5,27). This has led to a picture in which dimers or trimers of very close-lying pigments equilibrate on a very fast subpicosecond timescale, followed by transfer between clusters on the stromal and luminal sides. The isolated position of a Chl *b* (b605 in the Liu nomenclature (14)) and a Chl *a* (a604) molecule in the structure (Fig. 1) leads to very slow transfer from and to these pigments, so-called bottleneck states, with transfer times of ~1–3 ps and 40 ps, leading to a population and depopulation of a604 in 0.5–1 ps and 10–20 ps, respectively (5).

To provide a direct link between spectroscopic data, reporting on the dynamics of energy transfer and crystallographic data and then reporting on the structure of LHCII, we have performed time-resolved visible-pump/mid-infrared (IR) probe measurements on trimeric LHCII complexes. So far, to our knowledge, no ultrafast infrared measurements have been reported for LHCII. Time-resolved infrared spectroscopy is a highly specific technique, able to give information on the connection between the dynamics of energy transfer in proteins and specific structural details, as it is sensitive to subtle variations in bond length and angle changes. Signals in the infrared are often of small intensity, which means that, to assign specific signatures, the spectral information has to be compared with data previously available from different experimental techniques and from theoretical modeling. The data

Submitted April 7, 2009, and accepted for publication September 15, 2009.

*Correspondence: ml.groot@few.vu.nl

Editor: Feng Gai.

0006-3495/09/12/3215/9 $2.00

doi: 10.1016/j.bpj.2009.09.037

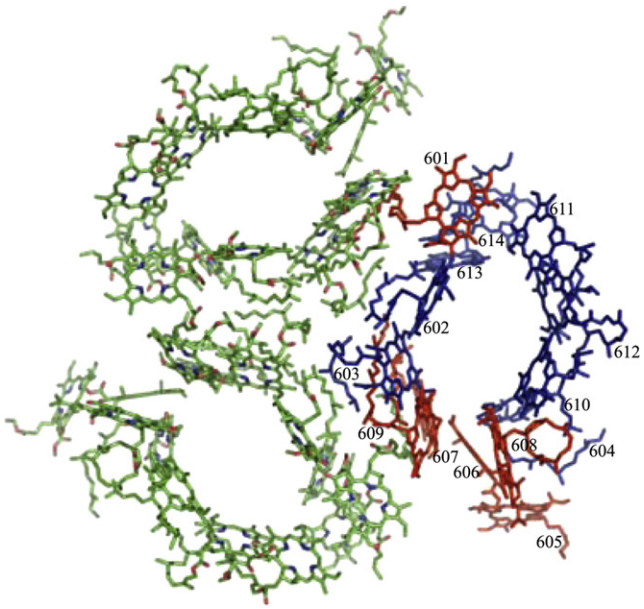

FIGURE 1 LHCII trimer: View from the top. Chl *a* values are colored in blue and Chl *b* values are red, for one out of the three monomeric subunits. Amino acids and carotenoids are not shown.

obtained with time-resolved infrared spectroscopy are, however, of sufficient resolution for us to recognize specific dynamic changes, as demonstrated in our previous work on the reaction centers proteins and PSII core complexes (28–31). Importantly, with infrared spectroscopy we can make the connection between dynamics and structure, which cannot be done with any other technique.

In this work, we have studied the 1600–1800 cm^{-1} spectral range. This region probes mainly the absorption changes in the C=O stretches of the chromophore (and protein), i.e., the 13^1-keto and 13^2-ester modes, and a mode sensitive to the macrocycle structure. The keto and ester modes are sensitive to the presence and strength of hydrogen bonds that the Chl may engage at these positions with the protein. Energy transfer between pigments having different strengths of hydrogen bonds with the protein should therefore show up as time-dependent absorption changes in the region of the 13^1-keto and 13^2-ester bands. Furthermore, we have used selective excitation wavelengths to assign ground-state bleached bands pertaining to Chls *b* and Chls *a* molecules and to better disentangle the energy transfer dynamics. By connecting the information obtained from the analysis of infrared data with the structural data from the crystal structure of LHCII, it is therefore possible to link the flow of excitation energy to the response of specific molecules in the structure. We also recorded induced electronic absorption changes in the Q_Y spectral region of the Chls. This facilitates recognizing the contribution of the Chl *b* and of the Chl *a* pigments in the spectra, and allows us to determine the extent of excitation-excitation annihilation present in the visible-midIR experiments. We had previously applied this approach to study the dynamic-structure relation in the core antenna complexes of PSII, CP43, and CP47 (30,31). One of the principal points of our article concerns the assignment of a specific infrared signature to the bottleneck state in the energy transfer dynamics of LHCII, indicated by previous modeling studies as Chl a604.

MATERIALS AND METHODS

Sample preparation

The isolation of LHCII trimers particles has been carried out as described in Leeuwen et al. (32) with some modifications. PSII membranes were diluted in BTS400 buffer: 20 mM Bis-Tris (pH 6.5) (Sigma-Aldrich Chemie BV, Zwijndrecht, The Netherlands), 20 mM $MgCl_2$ (Merck KGaA, Darmstadt, Germany), 5 mM $CaCl_2$ (Merck KGaA), 10 mM $MgSO_4$ and 0.4 M sucrose to a concentration of 2 mg Chl/mL. A 1:7 volume of a 10% (w/v) beta-dodecyl maltoside (β-DM, Anatrace, Maumee, OH) solution in BTS400 was added to a final concentration of 1.25% (w/v) detergent and 1.75 mg Chl/mL. The suspension was incubated at room temperature for 20 min, while being gently stirred. By centrifugation for 20 min at 40.000 $\times$ *g*, the nonsolubilized material was removed. The supernatant was then transferred to a Q-Sepharose column (1 g dry weight/mg Chl; Pharmacia, St. Paul, MN), equilibrated with $BTS400^+$ and β-DM 0.03%. A step gradient of 20 and 100 mM $MgSO_4$ (Merck KGaA) in the same buffer allowed separation of the Photosystem II core complex and of the LHCII. The LHCII enriched eluate was diluted and applied on a continuous sucrose gradient to separate trimers and monomers. A quantity of 0.5 M sucrose in BTT buffer (20 mM Bis-Tris, pH 6.5, 20 mM $MgCl_2$, 5 mM $CaCl_2$, and 10 mM $MgSO_4$) was frozen and thawed at room temperature to create the gradient. The separation occurred during centrifugation for 17 h at 40,000 rpm at 4°C (32).

The buffer was replaced with a D_2O (Merck KGaA) buffer (20 mM Bis-Tris, 20 mM NaCl, and 10 mM $MgCl_2$, 0.03% (w/v) β-DM at a pD of 7) for the infrared experiments. The absence of H_2O from the final preparation was checked by recording a steady-state Fourier transform infrared spectrum. A three-component oxygen scavenger (5 mM glucose, 0.1 mg/mL glucose oxidase, and 0.05 mg/mL catalase (Sigma-Aldrich Chemie BV)) was added to suppress the formation of radical oxygen and thereby any damage to the sample. The concentration of free monomers in the sample was $\leq$10% as judged from size-exclusion chromatography, using a Superdex model No. 200 HR 10:30 (Pharmacia) in a *fast protein liquid chromatography* system equipped with a diode array detector (Shimadzu, Columbia, MD). The composition of the buffer used as the mobile phase was 20 mM Bis-Tris, pH 6.5, 5 mM $MgCl_2$, and 0.03% β-DM. The sample was placed in a cell consisting of two CaF_2 windows separated by a spacer of 20 μm. The optical density was measured to be 0.5:20 μm at the Q_Y region of Chl *a*.

Experimental setup

The transient absorption experiments in the visible and mid-IR spectral ranges were performed with a setup described in more detail in Groot et al. (33). Briefly, the output of a Ti:Sapphire regenerative-amplified laser system operating at 1 kHz (Hurricane; SpectraPhysics, Mountain View, CA) is divided in three beams. One beam was sent to a homebuilt noncollinear optical parametric amplifier (NOPA) system to generate the excitation pulse at the desired center wavelengths of 650, 660, and 675 nm. A narrow bandwidth (11.5 nm, full width at half-maximum at 650 nm; 5 nm, full width at half-maximum at the other wavelengths) and high conversion efficiency in the NOPA were obtained by placing an appropriate interference filter in the path of the white-light seed of the NOPA. The second beam was sent into a traveling-wave optical parametric amplifier of superfluorescence (TOPAS, light conversion) equipped with difference frequency-generation to generate the probe pulse, with a central wavelength of 5952 nm (1680 cm^{-1}). With the third beam, a white light continuum was generated by focusing it on a 2-mm

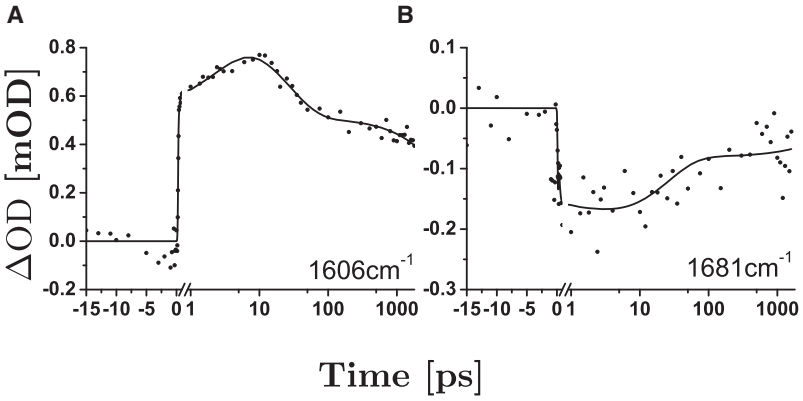

FIGURE 2 Representative time traces of LHCII recorded upon excitation at 650 nm, with fits derived from global analysis of the data over the full 1750–1600 cm^{-1} spectral range.

quartz plate. The excitation pulse from the NOPA was focused in the sample to a diameter of ~130 μm, and spatially overlapped with either of the two probe beams. The absorption changes in the visible were recorded after dispersion in a spectrograph, with a 256-element diode array (model No. S4801-256Q; Hamamatsu, Hamamatsu City, Japan); those in the mid-IR after dispersion, with a 32-element mercury cadmium telluride detector array (InfraRed Associates, Stuart, FL).

For the mid-IR experiments, two different gratings were used, resulting in a per-channel resolution of 3 cm^{-1} and 6 cm^{-1}, respectively. The pump beam was polarized at the magic angle orientation (54.7°) with respect to each probe beam with a Berek polarizer. The sample was moved during the measurement in a Lissajous scanner to ensure a fresh spot for every excitation pulse. A phase-locked chopper operating at 500 Hz was used to ensure that every other shot the sample was excited and the changes in transmission and hence optical density could be measured. The time delay between pump and probe beams was controlled by sending the pump beam over a moveable delay line.

The instrument response function for both variants of the setup, determined via the cross-correlation of pump and probe was ~150 fs. The energy per pulse for the mid-IR measurements was set to ~80–100 nJ, for the visible/visible measurement pulse energies of 5, 25, 50, 75, 100, and 120 nJ were used. All measurements were performed at room temperature. The sample concentration for all measurements was ~0.5 optical density for a 20-μm path length at 675 nm.

Data analysis

The transient data were analyzed using a global fitting routine as described in Leeuwen et al. (34). For each excitation wavelength, a set of 150 scans for all 32 channels was averaged and 69 time points per scan were taken. Each time point is the average value of 500 laser pulses. All the collected datapoints were analyzed together. The signal/noise ratio of all measurements performed was >5:1.

RESULTS

Visible pump/mid-IR probe measurements

Time-resolved visible pump/mid-IR probe measurements were performed by using three different excitation wavelengths: 650 nm preferentially exciting Chl *b* pigments; 675 nm preferentially exciting Chl *a* molecules; and an intermediate less-specific 660-nm excitation wavelength. Two representative time traces measured at 1606 and 1681 cm^{-1} upon excitation of LHCII trimers at 650 nm, with a power of ~100 nJ are shown in Fig. 2, *A* and *B*. The line through the data is a fit with time constants of 0.2 ps, 3 ps, 27 ps, and a long-lived component, and a (Gaussian) component that follows the instrument response function instantaneously (not shown). The latter describes the coherent interaction of the laser pulses in the sample and will not be further discussed here.

650-nm excitation

Using the 650-nm excitation wavelength, data were collected with a spectral resolution of 6 cm^{-1} and with a higher 3 cm^{-1} resolution in two smaller, partially overlapping, spectral windows. All time traces collected in the region 1750–1590 cm^{-1} are well fitted with the four time constants of 0.2 ps, 3 ps, 27 ps, and a nondecaying component. Fig. 3 shows the spectral evolution of the time-dependent absorption changes when fitted to a sequential model (state 1, state 2, state 3, state 4) yielding evolution-associated difference spectra (EADS) (34). In the EADS representing the initial spectral component (Fig. 3, *black line*) we observe the

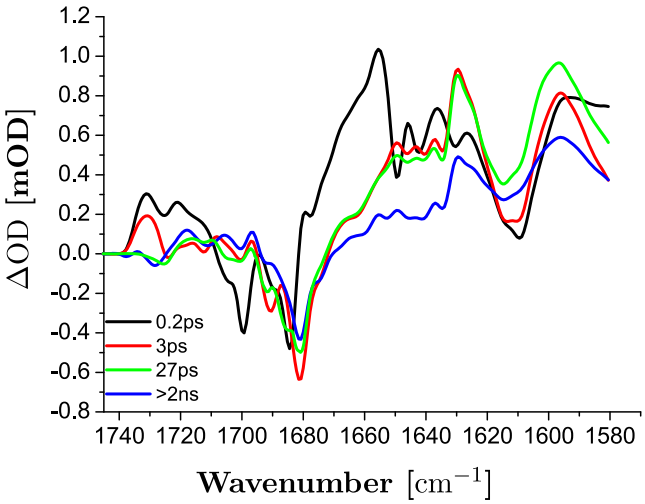

FIGURE 3 Evolution-associated difference spectra of LHCII upon 650-nm excitation. This plot was generated by combining the EADS recorded with 3 cm^{-1} resolution, taken in two measurements centered at 1680 and 1710 cm^{-1} with 100 cm^{-1} width and one measurement with 6 cm^{-1} resolution for the whole range centered at 1680 cm^{-1}. This results in a 3-cm^{-1} resolution between 1730 and 1650 cm^{-1} and 6 cm^{-1} at the extremes.

bleaching of two keto 13^1C=O modes of Chl *a* or *b* molecules at 1701 and 1682 cm^{-1} plus an excited state absorption band extending from ~1670 to 1620 cm^{-1}. This positive feature presents several peaks, the most intense of them at ~1650 cm^{-1}. Note that the 0.2-ps component is close to our instrument response function and may be affected by perturbed free induction decay (35). However, we attach significance to this spectral component, because it is absent when excitation at 660 and 675 nm is used (see below).

The exact frequency of the keto stretch of a chlorophyll molecule depends on whether or not it has a hydrogen bond and on the polarity of its environment. The stronger the hydrogen bond, or the larger the polarity of the environment, the lower the frequency of the 13^1 C=O mode. The positive absorption difference signal at <1670 cm^{-1} is due to the downshift of the 13^1 keto C=O stretch in the excited state. A similar shift to lower frequencies was observed for the excited state of Chls *a* in the CP43 and CP47 antenna complexes (30,31) and in the photosystem II reaction center (28). In tetrahydrofuran (in which Chl is in a non-hydrogen-bonded form) the keto stretch of Chl *a* downshifts from 1695 to 1660 cm^{-1} and that of Chl *b* from 1700 cm^{-1} to 1650 cm^{-1} (see Fig. 4). In LHCII, the bleached bands change in amplitude and shift in time, indicating the bleaching of different sets of Chl *a* and *b* molecules as the energy transfer progresses (Fig. 3). After 200 fs, the spectrum (represented by the *red line* in Fig. 3), living for 3 ps, appears. Here we mainly see an overall decay of the excited state absorption band, an almost complete recovery of the 1701 cm^{-1} bleached band and the appearance of two different bleached signals, at 1692 and 1680 cm^{-1}. In the following evolution (Fig. 3, *red* to *green line*), we mainly see an increased population of pigment(s) with a keto mode at 1685 cm^{-1} and a slight recovery of all the other bleached modes. Finally, the green spectrum decays in 27 ps into the blue component, living for >2 ns, where we observe a further minor decay for the bleach at ~1680 cm^{-1} and a 50% loss (as compared to the initial component) in the excited-state absorption at 1630 and 1600 cm^{-1}.

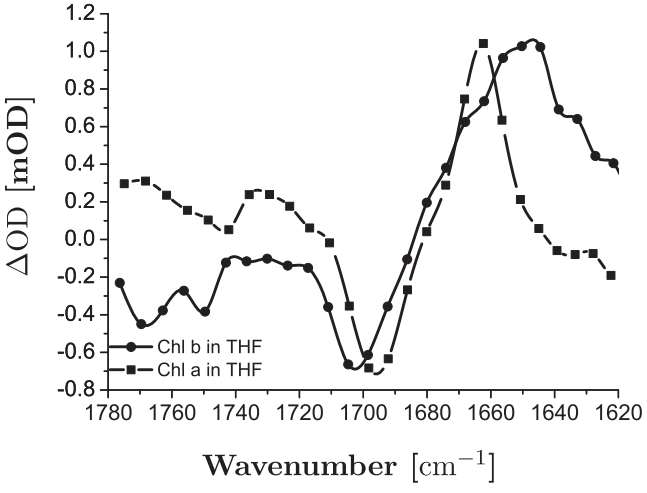

FIGURE 4 Chl *a* and *b* in tetrahydrofuran (THF), normalized EADS of a 2-ns lifetime component. The major bleach at ~1700 cm^{-1} is due to the 13^1-keto group vibration in the ground state. Upon formation of the excited state, this mode downshifts to 1660 cm^{-1}. Excitation wavelength was 450 nm for Chl *a* and 650 nm for Chl *b*.

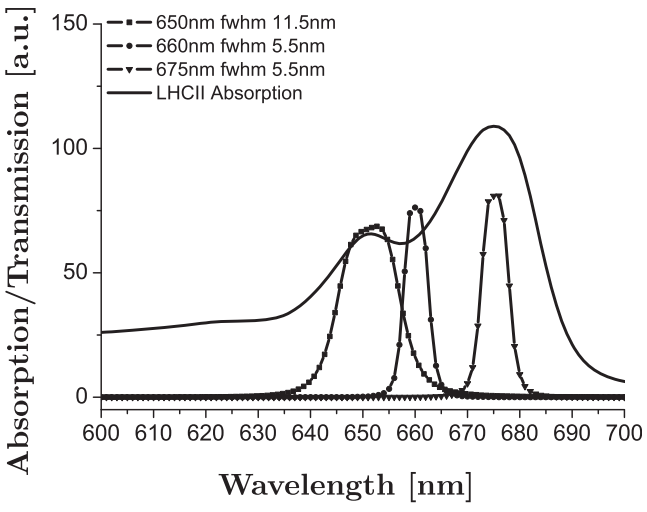

FIGURE 5 The absorption spectrum of trimeric LHCII complexes overlaid with the transmission spectra of the interference filters used to set the pump wavelength.

660- and 675-nm excitation

Upon 650 nm, for a large part, we directly excite the Chl *b* molecules. We collected data upon excitation at 660 and 675 nm to progressively excite more Chl *a* directly than Chl *b* (Fig. 5) shows the absorption spectrum of the LHCII trimers overlaid by the shape of the excitation pulses used. Each dataset was fitted with a set of 2–4 exponential decays. In Fig. 6 we compare the EADS with similar time constants obtained for the different excitation wavelengths with each other. The EADS of the longest-lived component (>1 ns, see Fig. 6 *D*) are very similar to each other, showing that, independently of the excitation wavelength, after ~30 ps an equilibrated state is reached. To offset the dynamics at earlier times from this equilibrium spectrum, we show the averaged nanosecond spectrum in each of the other panels.

In Fig. 6 *A*, the EADS of the first kinetic component are plotted; note that here the lifetime of the EADS range from 0.2 to 3 ps. Clearly, the band at 1701 cm^{-1}, highlighted in gray, and possibly that at 1682 cm^{-1}, highlighted in red, are typical for 650-nm excitation, and are therefore most likely due to a group of Chl *b* molecules. In the spectra obtained with 660- and 675-nm excitation, we observe bands at 1692 cm^{-1} (highlighted in *green*) and at 1680 cm^{-1} (highlighted in *orange*). In Fig. 6 *B*, we then compare the EADS of the following lifetime component (note that for 675-nm excitation, we plot the 3-ps spectrum once more). There is a relatively large resemblance of the ~3:6 ps EADS with the >1-ns averaged spectrum. Surprisingly, however, the EADS of the next phase, living for ~30 ps (Fig. 6 *C*), show

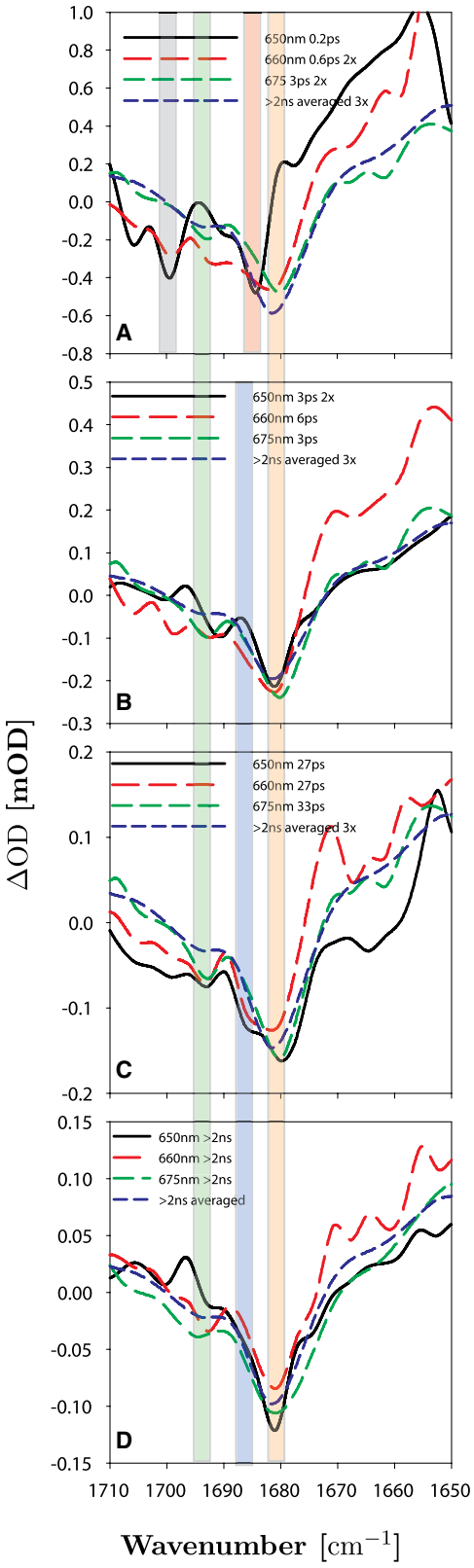

FIGURE 6 Mid-IR absorption difference spectra of LHCII recorded with 3 cm^{-1} resolution, upon excitation at 650, 660, and 675-nm excitation grouped such that the <1 ps (*A*), ~3 ps (*B*), >25 ps (*C*), and >2 ns (*D*) EADS are comparable. Regions of interest highlighted: 1680 cm^{-1}, orange; 1682 cm^{-1}, red; 1685 cm^{-1}, blue; 1692 cm^{-1}, green; and 1701 cm^{-1}, gray. In panel *A*, spectra have been normalized to have the bleached bands at 1680 and 1701 cm^{-1} at the same amplitude.

a deviation from the equilibrated spectrum as an additional band at 1685 cm^{-1} (highlighted in *blue*). This band is depopulated in ~25–30 ps, leading to the final spectrum, with bleachings at 1692 cm^{-1} and 1680 cm^{-1}. The total decay of the signal within the timescale of the experiment (2 ns) is approximately a factor of 3–6. The main loss takes place in the first few 100 fs and is mainly due to annihilation (see below for more discussion).

Visible pump/visible probe measurements

To obtain an independent measure of the amount of Chl *a* and *b* molecules excited at 650 nm, we collected transient pump-probe spectra in the visible region of the spectrum. In addition, the relatively small signals in the mid-IR spectral region necessitated the use of a pulse energy that probably resulted in an excitation density of >1 excitation per trimer. The visible transient signals were therefore recorded as a function of excitation power, to determine the extent to which excitation-excitation annihilation influenced the dynamics.

In Fig. 7, time traces recorded at 650 nm and 675 nm are shown for excitation energies of 5 nJ and 100 nJ. The time traces of each dataset were fitted simultaneously, using a sequential scheme with four decreasing rates. The corresponding EADS are shown in Fig. 8. The time constants obtained for all pulse energies are very similar: 0.25, 2.6 ps, 17 ps, and >1 ns. Only at the lowest excitation power of 5 nJ, two longer time constants are found for the first two components: 0.33 ps and 5 ps. The time-zero spectra show two bleaching signals centered at 650 nm and at 675 nm due to the ground-state bleach and stimulated emission of Chl *b* and Chl *a* molecules, respectively. The bleaching at $t = 0$ of the absorption at 675 nm may be due to ultrafast Chl-*b*-to-*a* energy transfer occurring within our instrument response function (~130 fs) and to direct excitation of Chl *a* molecules at 650 nm via vibronic transitions. At 5 nJ, the fast decay in amplitude for the 650-nm bleach, in conjunction with the rise at 675 nm, indicates Chl-*b*-to-Chl-*a* transfer with a time constant of 0.33 ps. A small fraction of Chl *b* molecules remains populated and transfers its excitation energy after 5 ps. However, this does not result in a gain of signal at 675 nm, probably because of compensation by excitation annihilation among Chl *a* pigments on this timescale, showing that even at the lowest pulse energy, we are not annihilation-free. Indeed, the next spectral evolution, occurring in 17 ps, shows an almost 50% reduction of signal. The spectral evolution at higher pulse energies is up to a factor-of-2 faster, except for the 17-ps component, and consists of a progressive decay of the signal.

As it can be observed in Fig. 8, the spectral shape of the signal obtained with higher excitation energies is different

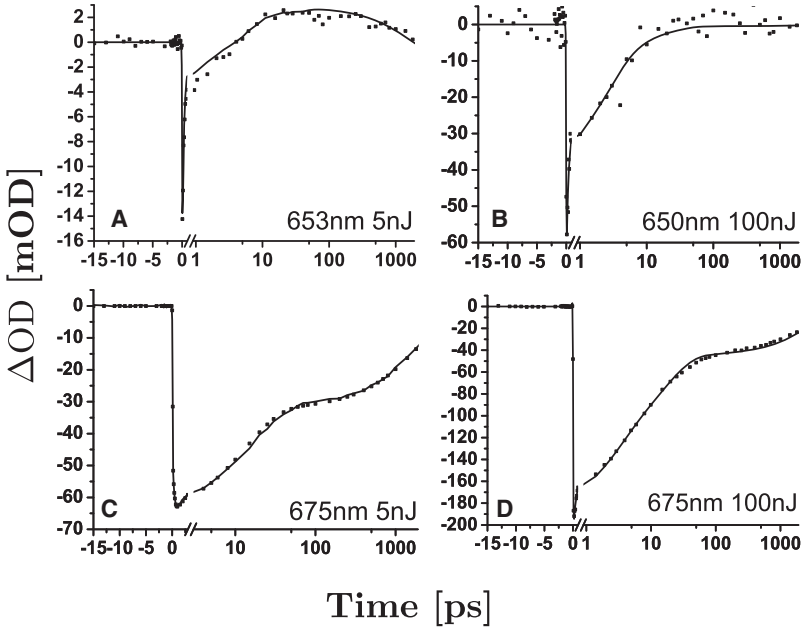

FIGURE 7 Four representative time traces of LHCII recorded at 650 and 675 nm upon excitation at 650 nm with excitation powers of 5 and 100 nJ. Timescale is linear up to 0.9 ps for panels *A*, *B*, and *D*; up to 3 ps for panel *C* to accentuate the fastest component, and logarithmic from thereon.

from that at 5 nJ. In all cases there is a higher contribution of the signal at 660–665 nm (the *blue side* of Chl *a* absorption) on the picosecond timescales and the appearance of an excited-state absorption band at <630 nm for the ~0.26 ps and 2.6 ps EADS. We furthermore note that the second EADS are clearly red-shifted with respect to the first and third ones and that there is a gain of signal at ~685 nm in the last spectral component (see Fig. 8). Similar observations, consisting of a dynamic blue shift followed by a red shift of the absorption difference signal in the Chl *a* Q_Y region at high excitation densities, were made for the antenna complexes CP43 and CP47 (30,31), for aggregates of protochlorophyllide in H_2O (O. Sytina, V. Novoderezhkin, R. van Grondelle, and M. L. Groot, unpublished data), and in the bacterial light harvesting system, LH2 (36). These observations are probably due to the population of multiexciton states, as a result of the high excitation density (36). More elaborated research on this specific topic is currently carried out in our group.

DISCUSSION

The timescale of the dynamics in LHCII in the mid-IR spectral range is similar to that in the visible region. The visible transient spectra collected as a function of the pulse energy show that with the excitation power used in the mid-IR, multiple excited states are created in one complex, and that annihilation of these excited states leads to a net loss of

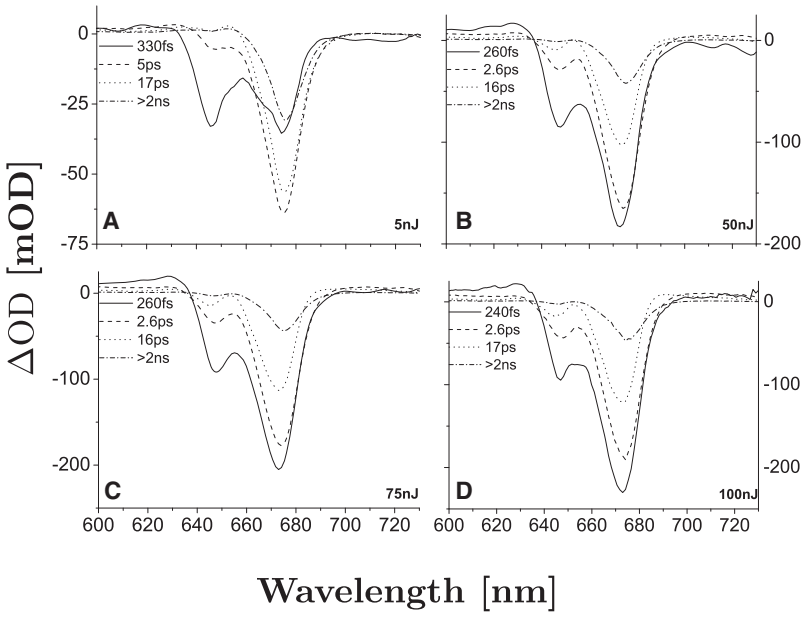

FIGURE 8 Absorption difference spectra of LHCII recorded between 600 and 730 nm upon excitation at 650 nm. Excitation energy per pulse: 5 nJ (*A*), 25 nJ (*B*), 50 nJ (*C*), and 100 nJ (*D*).

TABLE 1 Comparison of integrated areas of each EADS as measure of the amount of annihilation

Pump power [nJ]	$\frac{A\tau_1}{A\tau_2}$	$\frac{A\tau_2}{A\tau_3}$	$\frac{A\tau_3}{A\tau_4}$	$\frac{A\tau_1}{A\tau_{>2ps}}$
5	1	1.3	2	2.6
25	1.3	1.9	2.1	5.3
50	1.4	1.9	2.5	6.9
75	1.4	1.9	2.5	6.9
100	1.4	2	2.6	7.3

signal. The fact that excitation-annihilation leads to an acceleration of the observed energy transfer times (5,37) is in line with the observation of a decrease of the first time constant from 0.33 fs to 0.25 fs, and of the second time constant from 5 ps to 2.6 ps. Furthermore, the net loss of signal in the mid-IR (a factor of ~3, see Fig. 3) is in line with the observed amount of annihilation in the visible absorption difference spectra. We have computed the relative amount of annihilation associated with each time constant by dividing the areas of the absorption difference spectrum for each pair of time constants (results are reported in Table 1). The visible spectra show, upon using excitation densities >5 nJ, some spectral features that may be ascribed to transitions from multiexciton levels are observable. We note additional intensity in the Chl *a* Q_Y region (675 nm) in the first component and a dynamic blue shift followed by a red shift of the signal. In the mid-IR, we expect, in first-order, not to see multiexciton effects on the bleached carbonyl modes.

Assignments of the IR bands to specific Chl a and b molecules

Using the crystal structure of LHCII we can obtain an assignment for the bleached signals observed in our spectra. We will compare this assignment with the results of a modeling study on the dynamics of energy transfer in LHCII based on the Redfield theory (5,27). Crystallographic data suggest that several chlorophyll molecules are in close enough contact with protein residues and structural water molecules to be engaged in hydrogen bonds via their C=O groups. In Table 2 we have collected a list of the hydrogen-bond partners of these pigments as found in Liu et al. (38). In the EADS of the initial kinetic component obtained by exciting the sample with a 650-nm pulse (see Fig. 6 *A*), two bleaching bands at 1701 cm^{-1} and 1682 cm^{-1} can be observed. This spectrum is clearly different from the initial spectra obtained upon excitation of the Chl *a* molecules. The combination of our broad excitation pulse, and fast ~100 fs energy redistribution among several of the Chl *b*s, as suggested in the literature (5,27), makes it likely that all Chl *b* molecules participate in the 0.2 ps EADS. However, in the visible we see a Chl *a* contribution already in the first component, which means that the 1701- and 1682-cm^{-1} band must be assigned to Chl *b* but partially also to blue-absorbing Chl *a* pigments. The high frequency of the 1701-cm^{-1} band is an indication that this keto group is free of hydrogen-bond interactions. The Chls *b* indicated as b601, b605, b606, and b607 have no H-bonding partner, and could therefore all contribute to the 1701-cm^{-1} band. There are two Chl *b*s with an H-bond: His-68 ND1 binds to Chl-b609 and Chl-b608 has an even stronger H-bond to Arg-70 NH1. Putative Chl *a* candidates who might contribute in this region to a small extent are Chl a602 with two H-bonds to Try-44 N and Trp-46 N, and a604 to an even smaller extent with its H-bond to Leu-113 N (38).

TABLE 2 List of chlorophyll molecules that have a H-bond partner to their 13^1-keto group according to Liu et al. (38)

Chlorophyll	H-bond partner to the 13^1-keto group
a602	Try-44 N, Trp-46 N
a603	Water
a604	Leu-113 N
b608	Arg-70 NH1
b609	His-68 ND1
b610	Gly-158 N

The second EADS, for all excitation wavelengths, is fairly similar to the long-term equilibrated spectrum (see Fig. 6 *B* in comparison with Fig. 6 *D*). However, after 3–6 ps, we see that spectral dynamics still occurs since a significant extra population of a (group of) pigment(s) with a keto band at 1685 cm^{-1} is then created (Fig. 6 *C*, *blue marked band*). This band decays after ~30 ps, and an equilibrated spectrum is formed that is constant up to the nanosecond timescale. The Redfield modeling studies (5,27) suggest the population of a bottleneck in the energy transfer process on this timescale, formed by Chl a604. The transient population of the 1680-cm^{-1} band can be identified with this pigment as, from the crystal structure, it appears that Chl a604 can indeed participate in a hydrogen bond, as it is at a short distance from Leu-113 N (38), which would agree with a downshifted position for its carbonyl absorption at 1685 cm^{-1}. The population and depopulation times to and from this pigment found in this study coincide reasonably well with those obtained in the Redfield modeling of various spectroscopic data (5,27), of Chl a604 population in 1 ps and depopulation in ~20 ps. Note that although this process is clearly resolved in the mid-IR data, in our own and in previously reported (5,16–26) visible pump-probe data, only a decay of amplitude is observed, without a specific spectral signature.

The final spectrum is characterized by the bleaching of one main band at 1680 cm^{-1}, and a second minor band at 1692 cm^{-1} (*orange* and *green marked bands* in Fig. 6 *D*). According to the Redfield model, in the final equilibrated state, a predominant population of the a610-a611-a612 cluster (mostly a610) is reached (5,16). Chl a610 can be engaged in a hydrogen bond to Gly-158 N, justifying the low frequency of the 1680 cm^{-1} band. The other pigments, a611 and a612 do not have a hydrogen bond, and may therefore be responsible for the band at 1692 cm^{-1} with the reduced amplitude, reflecting the lower population of these two pigments relative

to a610. The location of this cluster on the outer side of the LHCII trimer is likely to provide a good connection with the other subunits of PSII.

CONCLUSION

By applying femtosecond infrared spectroscopic measurements on LHCII we have provided a direct link between spectroscopic data, reporting on the dynamics of energy transfer, and crystallographic data, reporting on the structure of LHCII. Combination of our data with the results from the Redfield model and the information derived from the crystal structure of LHCII provides a unique visualization of the flow of energy through LHCII, and provides experimental support for the role of pigment Chl a604 as a bottleneck state.

We thank Henny van Roon and Sandrine d'Haene for sample preparation and biochemical characterization and Jos Thieme for his support and help with the experimental apparatus.

REFERENCES

1. Ogawa, T., F. Obata, and K. Shibata. 1966. Two pigment-proteins in spinach chloroplasts. *Biochim. Biophys. Acta.* 112:223–234.
2. Thornber, J. P., C. A. Smith, and J. L. Bailey. 1966. Partial characterization of two chlorophyll-proteins complexes isolated from spinach-beet chloroplasts. *Biochem. J.* 100:14.
3. van Grondelle, R. 1985. Excitation energy transfer, trapping and annihilation in photosynthetic systems. *Biochim. Biophys. Acta.* 811: 147–195.
4. van Grondelle, R., J. P. Dekker, T. Gillbro, and V. Sundstrom. 1994. Energy-transfer and trapping in photosynthesis. *Biochim. Biophys. Acta Bioenergetics.* 1187:1–65.
5. van Grondelle, R., and V. I. Novoderezhkin. 2006. Energy transfer in photosynthesis: experimental insights and quantitative models. *Phys. Chem. Chem. Phys.* 8:793–807.
6. van Amerongen, H., and R. van Grondelle. 2001. Understanding the energy transfer function of LHCII, the major light-harvesting complex of green plants. *J. Phys. Chem. B.* 105:604–617.
7. Horton, P., A. V. Ruban, and R. G. Walters. 1996. Regulation of light harvesting in green plants. *Annu. Rev. Plant Physiol. Plant Mol. Biol.* 47:655–684.
8. Niyogi, K. K. 1999. Photoprotection revisited: genetic and molecular approaches. *Annu. Rev. Plant Physiol. Plant Mol. Biol.* 50:333–359.
9. Horton, P., A. V. Ruban, and R. G. Walters. 1994. Regulation of light harvesting in green plants (indication by nonphotochemical quenching of chlorophyll fluorescence). *Plant Physiol.* 106:415–420.
10. Elrad, D., K. K. Niyogi, and A. R. Grossman. 2002. A major light-harvesting polypeptide of photosystem II functions in thermal dissipation. *Plant Cell.* 14:1801–1816.
11. Ruban, A. V., R. Berera, C. Ilioaia, I. H. M. van Stokkum, J. T. M. Kennis, et al. 2007. Identification of a mechanism of photoprotective energy dissipation in higher plants. *Nature.* 450:575–578.
12. Pascal, A. A., Z. F. Liu, K. Broess, B. van Oort, H. van Amerongen, et al. 2005. Molecular basis of photoprotection and control of photosynthetic light-harvesting. *Nature.* 436:134–137.
13. Allen, J. F., and A. Nilsson. 1997. Redox signaling and the structural basis of regulation of photosynthesis by protein phosphorylation. *Physiol. Plant.* 100:863–868.
14. Liu, Z., H. Yan, K. Wang, T. Kuang, J. Zhang, et al. 2004. Crystal structure of spinach major light-harvesting complex at 2.72 Å resolution. *Nature.* 428:287–292.
15. Standfuss, J., A. C. Terwisscha van Scheltinga, M. Lamborghini, and W. Kuhlbrandt. 2005. Mechanisms of photoprotection and nonphotochemical quenching in pea light-harvesting complex at 2.5 A resolution. *EMBO J.* 24:919–928.
16. Palacios, M. A., J. Standfuss, M. Vengris, B. F. van Oort, I. H. M. van Stokkum, et al. 2006. A comparison of the three isoforms of the light-harvesting complex II using transient absorption and time-resolved fluorescence measurements. *Photosynth. Res.* 88:269–285.
17. Kleima, F. J., C. C. Gradinaru, F. Calkoen, I. H. M. van Stokkum, R. van Grondelle, et al. 1997. Energy transfer in LHCII monomers at 77K studied by sub-picosecond transient absorption spectroscopy. *Biochemistry.* 36:15262–15268.
18. Visser, H. M., F. J. Kleima, I. H. M. van Stokkum, R. van Grondelle, and H. van Amerongen. 1996. Probing the many energy-transfer processes in the photosynthetic light-harvesting complex II at 77K using energy-selective sub-picosecond transient absorption spectroscopy. *Chem. Phys.* 210:297–312.
19. Linnanto, J., J. Martiskainen, V. Lehtovuori, J. Ihalainen, R. Kananavicius, et al. 2006. Excitation energy transfer in the LHC-II trimer: a model based on the new 2.72 Å structure. *Photosynth. Res.* 87:267–279.
20. Palsson, L. O., M. D. Spangfort, V. Gulbinas, and T. Gillbro. 1994. Ultrafast chlorophyll b-chlorophyll a excitation energy transfer in the isolated light harvesting complex, LHC II, of green plants: implications for the organization of chlorophylls. *FEBS Lett.* 339:134–138.
21. Bittner, T., K.-D. Irrgang, G. Renger, and M. R. Wasielewski. 1994. Ultrafast excitation energy transfer and exciton-exciton annihilation processes in isolated light harvesting complexes of Photosystem II (LHCII) from spinach. *J. Phys. Chem.* 98:11821–11826.
22. Croce, R., M. G. Muller, R. Bassi, and A. R. Holzwarth. 2001. Carotenoid-to-chlorophyll energy transfer in recombinant major light-harvesting complex (LHCII) of higher plants. I. Femtosecond transient absorption measurements. *Biophys. J.* 80:901–915.
23. Salverda, J. M., M. Vengris, B. P. Krueger, G. D. Scholes, A. R. Czamoleski, et al. 2003. Energy transfer in light-harvesting complexes LHCII and CP29 of spinach studied with three pulse echo peak shift and transient grating. *Biophys. J.* 84:450–465.
24. Gradinaru, C. C., I. H. M. van Stokkum, A. A. Pascal, R. van Grondelle, and H. van Amerongen. 2000. Identifying the pathways of energy transfer between carotenoids and chlorophylls in LHCII and CP29. A multicolor, femtosecond pump-probe study. *J. Phys. Chem. B.* 104: 9330–9342.
25. Holt, N. E., J. T. M. Kennis, L. Dall'Osto, R. Bassi, and G. R. Fleming. 2003. Carotenoid to chlorophyll energy transfer in light harvesting complex II from *Arabidopsis thaliana* probed by femtosecond fluorescence upconversion. *Chem. Phys. Lett.* 379:305–313.
26. Kwa, S. L. S., H. Vanamerongen, S. Lin, J. P. Dekker, R. Vangrondelle, et al. 1992. Ultrafast energy-transfer in LHCII trimers from the Chl a/b light-harvesting antenna of Photosystem-II. *Biochim. Biophys. Acta.* 1102:202–212.
27. Novoderezhkin, V. I., M. A. Palacios, H. van Amerongen, and R. van Grondelle. 2005. Excitation dynamics in the LHCII complex of higher plants: modeling based on the 2.72 Ångstrom crystal structure. *J. Phys. Chem. B.* 109:10493–10504.
28. Groot, M. L., N. P. Pawlowicz, L. van Wilderen, J. Breton, I. H. M. van Stokkum, et al. 2005. Initial electron donor and acceptor in isolated Photosystem II reaction centers identified with femtosecond mid-IR spectroscopy. *Proc. Natl. Acad. Sci. USA.* 102:13087–13092.
29. Pawlowicz, N. P., M. L. Groot, I. H. M. van Stokkum, J. Breton, and R. van Grondelle. 2007. Charge separation and energy transfer in the Photosystem II core complex studied by femtosecond midinfrared spectroscopy. *Biophys. J.* 93:2732–2742.
30. DiDonato, M., R. vanGrondelle, I. H. M. vanStokkum, and M. L. Groot. 2007. Excitation energy transfer in the Photosystem II core antenna complex CP43 studied by femtosecond visible/visible and visible/mid-infrared pump probe spectroscopy. *J. Phys. Chem. B.* 111:7345–7352.
31. Groot, M. L., J. Breton, L. J. G. W. vanWilderen, J. P. Dekker, and R. vanGrondelle. 2004. Femtosecond visible/visible and visible/mid-IR

pump-probe study of the Photosystem II core antenna complex CP47. *J. Phys. Chem. B.* 108:8001–8006.

32. Leeuwen, P. J., M. C. Nieveen, E. J. Meent, J. P. Dekker, and H. J. Gorkom. 1991. Rapid and simple isolation of pure Photosystem II core and reaction center particles from spinach. *Photosynth. Res.* 28:149–153.
33. Groot, M. L., L. van Wilderen, and M. Di Donato. 2007. Time-resolved methods in biophysics. 5. Femtosecond time-resolved and dispersed infrared spectroscopy on proteins. *Photochem. Photobiol. Sci.* 6: 501–507.
34. van Stokkum, I. H. M., D. S. Larsen, and R. van Grondelle. 2004. Global and target analysis of time-resolved spectra. *Biochim. Biophys. Acta. Bioenergetics.* 1657:82–104.
35. Hamm, P. 1995. Coherent effects in femtosecond infrared spectroscopy. *Chem. Phys.* 200:415–429.
36. Bruggemann, B., and V. May. 2004. Exciton-exciton annihilation dynamics in chromophore complexes. II. Intensity dependent transient absorption of the LH2 antenna system. *J. Chem. Phys.* 120: 2325–2336.
37. Valkunas, L., and E. Skaistis. 1976. Exciton-exciton and exciton-electron interaction in luminescence spectra of 2-dimensional crystals. *Fizika Tverdogo Tela.* 18:2594–2598.
38. Liu, Z., H. Yan, K. Wang, T. Kuang, J. Zhang, et al. 2004. Crystal structure of spinach major light-harvesting complex at 2.72 Å resolution, supplemental information. *Nature.* 428:287–292.